

ORIGINAL RESEARCH

Open Access



Quantitative analysis of ^{99m}Tc -pertechnetate thyroid uptake with a large-field CZT gamma camera: feasibility and comparison between SPECT/CT and planar acquisitions

Benjamin Serrano^{1*} , Régis Amblard¹, Tiffany Beaumont², Florent Hugonnet³, Matthieu Dietz⁴, Frédéric Berthier⁵, Nicolas Garnier¹, Rémy Villeneuve¹, Valérie Nataf³, François Mocquot³, Christopher Montemagno⁶, Marc Faraggi³ and Benoît Paulmier³

*Correspondence:
bserrano@chpg.mc

¹ Medical Physics Department,
Centre Hospitalier Princesse
Grace, Monaco, Monaco

² Laboratoire d'évaluation de
la dose interne, Institut de
Radioprotection et de Sécurité
Nucléaire, Fontenay-aux-Roses,
France

³ Nuclear Medicine Department,
Centre Hospitalier Princesse
Grace, Monaco, Monaco

⁴ Nuclear Medicine Department,
Hospices Civils de Lyon, Lyon,
France

⁵ Department of Biostatistics,
Centre Hospitalier Princesse
Grace, Monaco, Monaco

⁶ Department of Medical Biology,
Centre Scientifique de Monaco,
Monaco, Monaco

Abstract

Purpose: The main objective of this study was to evaluate the ability of a large field Cadmium Zinc Telluride (CZT) camera to estimate thyroid uptake (TU) on single photon emission computed tomography (SPECT) images with and without attenuation correction (Tomo-AC and Tomo-NoAC) compared with Planar acquisition in a series of 23 consecutive patients. The secondary objective was to determine radiation doses for the tracer administration and for the additional Computed Tomography (CT) scan.

Methods: Cross-calibration factors were determined using a thyroid phantom, for Planar, Tomo-AC and Tomo-NoAC images. Then Planar and SPECT/CT acquisitions centered on the thyroid were performed on 5 anthropomorphic phantoms with activity ranging from 0.4 to 10 MBq, and 23 patients after administration of 79.2 ± 3.7 MBq of [^{99m}Tc]-pertechnetate. We estimated the absolute thyroid activity (A_{ThA}) for the anthropomorphic phantoms and the TU for the patients. Radiation dose was also determined using International Commission on Radiological Protection (ICRP) reports and VirtualDoseTMCT software.

Results: Cross-calibration factors were 66.2 ± 4.9 , 60.7 ± 0.7 and 26.5 ± 0.3 counts/(MBq s), respectively, for Planar, Tomo-AC and Tomo-NoAC images. Theoretical and estimated A_{ThA} for Planar, Tomo-AC and Tomo-NoAC images were statistically highly correlated ($r < 0.99$; $P < 10^{-4}$) and the average of the relative percentage difference between theoretical and estimated A_{ThA} were (8.6 ± 17.8) , (-1.3 ± 5.2) and (12.8 ± 5.7) %, respectively. Comparisons between TU based on different pairs of images (Planar vs Tomo-AC, Planar vs Tomo-NoAC and Tomo-AC vs Tomo-NoAC) showed statistically significant correlation ($r = 0.972$, 0.961 and 0.935 , respectively; $P < 10^{-3}$). Effective and thyroid absorbed doses were, respectively $(0.34_{\text{CT}} + 0.95_{\text{NM}})$ mSv, and $(3.88_{\text{CT}} + 1.74_{\text{NM}})$ mGy.

Conclusion: A_{ThA} estimation using Planar and SPECT/CT acquisitions on a new generation of CZT large-field cameras is feasible. In addition, TU on SPECT/CT

was as accurate as conventional planar acquisition, but the CT induced additional thyroid exposure.

Trial registration Name of the registry: Thyroid Uptake Quantification on a New Generation of Gamma Camera (QUANTHYC). Trial number: NCT05049551. Registered September 20, 2021—Retrospectively registered, <https://clinicaltrials.gov/ct2/show/record/NCT05049551?cntry=MC&draw=2&rank=4>.

Keywords: Thyroid, Absolute activity, Uptake, Quantification, CZT, Planar, SPECT/CT

Background/introduction

For more than 50 years, sodium ^{99m}Tc -pertechnetate ($^{99m}\text{TcO}_4$) has been used to assess thyroid function and thyroid uptake by planar thyroid scintigraphy [1–6]. $^{99m}\text{TcO}_4$ has been used worldwide for thyroid gland examination because it has a short half-life (6 h) compared to ^{131}I -Iodide (8 days) and because it does not produce beta radiation, providing a low overall radiation dose to the gland [7]. ^{123}I -Iodide has similar advantages to $^{99m}\text{TcO}_4$ in planar scintigraphy, namely a short half-life (13 h) and a gamma-ray emission of 159 keV compared to the 140 keV of ^{99m}Tc , both of which are suitable for an Anger camera. However, cost and availability factors have made $^{99m}\text{TcO}_4$ preferred over ^{123}I -Iodide.

Positron Emission Tomography (PET) with ^{124}I has recently been presented as a valuable clinical tool for the exploration of patients with thyroid disease [8, 9]. Darr et al. [10] performed a blinded pilot comparison between PET with ^{124}I and planar $^{99m}\text{TcO}_4$ scintigraphy or its cross-sectional enhancement single photon emission computed tomography (SPECT) for thyroid characterization. The conclusion of the study provides superior imaging of PET with ^{124}I due to higher spatial resolution. However, the lack of commercial availability of the tracer, the potential cost of ^{124}I and the need to use a PET camera are significant limitations compared to $^{99m}\text{TcO}_4$.

Tomographic acquisitions (SPECT and SPECT/CT) are powerful diagnostic tools that improve the diagnostic quality of conventional planar scintigraphy which is currently the gold standard. Absolute quantitative analysis has proven to be achievable in SPECT/CT [11–14], thanks to technical improvements such as iterative reconstruction, scatter correction, computed tomography (CT) attenuation correction and resolution recovery [15, 16].

A new generation of gamma cameras with Cadmium Zinc Telluride (CZT) dual detectors with a large field of view have recently emerged. These cameras offer better spatial and energy resolutions than NaI scintillator detector [17]. All-purpose CZT cameras have been introduced to the market, but they are not yet widely used to study thyroid disease. Our aim was to investigate thyroid quantification (absolute thyroid activity and thyroid uptake) in anthropomorphic phantoms and in patients with planar and SPECT imaging on a latest generation of CZT gamma camera, with and without attenuation correction using a low dose CT scanner. We also aimed to investigate the respective fraction of thyroid absorbed dose caused by the CT scan and the isotope administration.

Materials and methods

Data acquisitions

All acquisitions were performed using a dual-head gamma camera Discovery NM/CT 870 CZT (GE Healthcare, Milwaukee, WI, USA). The camera was equipped with a WEHR45 (Wide Energy High Resolution 45 mm length) low energy collimator adjusted

to the CZT detector element with pixel size of 2.46 mm. The collimator description is of a square hole type with a length of 45 mm, side of 2.26 mm and septal thickness of 0.2 mm. Clinical acquisition protocols for planar and SPECT/CT imaging are detailed below. The acquisition analysis was carried out on XELERIS 4.1 processing software (GE Healthcare) workstation with Q-Volumetrix MI post-treatment application. To date, there is no pinhole on this equipment.

Planar images over antero-posterior incidence of cervical region were acquired with the following camera settings: 256×256 matrix size, zoom factor of 3, acquisition time of 900 s and a photon energy window of $140 \text{ keV} \pm 10\%$. The pixel size was $0.74 \times 0.74 \text{ mm}^2$. The distance between the anterior head of the camera and the patients or phantoms was fixed at 12 cm. An advanced settings algorithm, called Clarity Zoom (GE Healthcare) was applied. It is described as a post-processing imaging enhancing system that works by filtering and resampling images with contrast enhancement. The planar acquisition was considered as the reference image for the thyroid uptake estimation in clinical practice [1–6, 18, 19].

Tomography acquisitions were performed with a 128×128 matrix size, a corresponding voxel size of $4.92 \times 4.92 \times 4.92 \text{ mm}^3$, 60 projections (30 per detector head), 20 s per projection and zoom factor 1. We used the option of acquiring during motion between steps inducing a total time acquisition of 700 s. An energy spectrum window of $140 \text{ keV} \pm 7.5\%$ and a scatter window of $120 \text{ keV} \pm 5\%$ were used. The autocontouring (body contour) option was selected to ensure a minimum distance between detectors and the phantoms or the patients. Data of SPECT images were reconstructed using an iterative Ordered Subsets Expectation Minimization (OSEM) reconstruction algorithm, 4 iterations and 6 subsets, which included resolution recovery reconstruction (RR) and scatter correction. A post-reconstruction filter was also applied: a Gaussian filter of 1.5 mm in *X*, *Y*, and *Z* directions. The attenuation correction was applied using the CT scanner, a 16-slice Optima CT540, for the Tomo-AC dataset. Another set of reconstructions was made with the same parameters but without attenuation correction (*Tomo-NoAC*).

CT images were acquired from the maxilla to the sternal manubrium using the following parameters: 100 kVp tube voltage, tube current modulated with Smart mA (GE Healthcare, Milwaukee, WI, USA), maximum 75 mA and noise index up to 30, rotating time 0.9 s, pitch 1.375, 512×512 matrix size and slice thickness of 1.25 mm. The voxel size was $0.98 \times 0.98 \times 1.25 \text{ mm}^3$. An iterative reconstruction algorithm, Adaptive Statistical Iterative Reconstruction (ASIR), (GE Healthcare, Milwaukee, WI, USA), was used for the data reconstruction.

Cross-calibration parameters of the CZT gamma camera

The cross-calibration factor was computed using the acquisition of known $^{99\text{m}}\text{Tc}$ activity in a standardized phantom, a Plexiglass cylindrical ANSI/IAEA (American National Standards Institute/International Atomic Energy Agency) neck thyroid phantom. The phantom's diameter and the height are 127 mm. Its thyroid simulator is a cylindrical hole on which a 15 ml vial is inserted. The acquisition and reconstruction parameters with the phantom were strictly the same as those used in clinical cases and described above. Only the vial contained radioactivity; the rest of the phantom was cold. The 20 mm depth at

the location of the center of the vial corresponds to the thyroid depth in the neck of an average adult person (Fig. 1).

To ensure the linearity of the cross-calibration factor with the injected ^{99m}Tc activity, various acquisitions were carried out in planar and tomographic modes, with radioactivity in the vial ranging from 1 to 20 MBq.

The cross-calibration factor F_{cal} in counts/(MBq.s) is given by:

$$F_{\text{cal}} = \frac{N_{\text{ROI}}}{A_{\text{acq}} * \Delta t}$$

where N_{ROI} is the number of counts in the region of interest and A_{acq} (MBq) is the mean activity of radioactivity decay in the vial over the acquisition duration Δt (s). Therefore, A_{acq} is given by the equation:

$$A_{\text{acq}} = \frac{A_0 \cdot \int_0^{\Delta t} e^{-(\ln 2) \cdot t / T} \cdot dt}{\Delta t}$$

where A_0 (MBq) is the initial activity, T (s) is the half-life of the ^{99m}Tc . The quantification of activity was performed in the same way for the patients. More precisely, volumes of interest (VOIs) for Tomo-AC and Tomo-NoAC, and the regions of interest (2D ROIs) for Planar, were automatically segmented using a threshold of 40% of P_{max} [20] for SPECT and SPECT/CT VOIs, and 25% of P_{max} for Planar ROIs. P_{max} is defined as the maximum counts in a voxel (or pixel) within the region. In a preliminary study to validate these threshold values, a vial mimicking thyroid fixation (diameter 2.2 cm and height of 4 cm) was acquired with SPECT and planar acquisitions. The VOIs and 2D ROIs obtained of the vial images, with thresholds of 40% of P_{max} and 25% of P_{max} , respectively, were in agreement with the vial's geometric characteristics.

Anthropomorphic phantom analysis

Five anthropomorphic thyroid phantoms manufactured by IRSN (Institut de Radioprotection et de Sûreté Nucléaire) were imaged using the cross-calibration factor



Fig. 1 Neck phantom for thyroid cross-calibration factor determination for the planar, SPECT/CT and SPECT acquisitions

determined above to estimate the absolute thyroid activity (A_{ThA}). The thyroid volumes in the five phantoms were selected at 3.2, 7.5, 11.4, 19 and 30 cc, in alignment with ICRP recommendations for thyroid volumes and were inserted inside a neck phantom that contained a replica spinal cord and vertebral column (Fig. 2). These phantoms were designed with a realistic anthropomorphic shape. The phantoms were 3D printed using specific materials for an accurate simulation of the attenuation of biological tissues [21]. The tomography and planar acquisitions and reconstructions parameters were exactly the same as those used in clinical cases and described above. The range of activity in the ^{99m}Tc solution injected into the thyroid phantoms was between 0.4 and 10 MBq. The theoretical absolute activity injected in the thyroid was defined as theoretical A_{ThA}. The estimation of the A_{ThA} was performed with the planar, Tomo-AC and Tomo-NoAC images.

The A_{ThA} was calculated as the following relation:

$$A_{ThA} \text{ (MBq)} = \frac{N_{ROI,th}}{F_{cal} * \Delta t}$$

where F_{cal} is the cross-calibration factor, Δt (s) the acquisition duration and $N_{ROI,th}$ the counts in thyroid that were automatically segmented in the same way as the cross-calibration factor was determined.

Measurement methodology of thyroid uptake

The thyroid uptake (TU) was calculated as the following relation:

$$TU (\%) = \frac{A_{th}}{A_i} * 100 = \frac{N_{ROI,th} - N_{back}}{F_{cal} \cdot A_i} * 100$$

where A_{th} (MBq) is the activity measured in the thyroid ROI or VOI, A_i (MBq) is the activity injected to the patient and F_{cal} is the cross-calibration factor. The actual injected activity A_i was calculated by subtracting the activities of the full syringes with the empty ones.

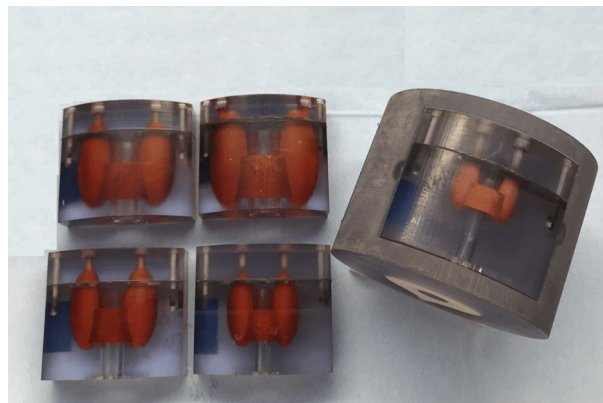


Fig. 2 Five anthropomorphic thyroid phantoms made by IRSN (Institut de Radioprotection et de Sûreté Nucléaire). The phantom volume were 3.2, 7.5, 11.4, 19 and 30 cc and were introduced in the anthropomorphic neck phantom

The activity in the thyroid A_{th} was estimated in three different ways: static planar, SPECT and SPECT/CT acquisitions. The regions of interest, in which the counts in thyroid $N_{ROI,th}$ were measured, were automatically segmented in the same way as for the determination of the cross-calibration factor: a threshold of 40% of P_{max} was chosen for the VOI on SPECT and SPECT/CT images, and a threshold of 25% of P_{max} was chosen for the 2D ROI on planar images. Additionally, a background region of interest (ROI_{back}) was drawn underneath the thyroid in order to obtain a background corrected 2D ROI Thyroid counts for planar acquisitions. This background region of interest was not applied for the SPECT images.

Then for SPECT acquisitions: $TU (\%) = \frac{N_{ROI,th}}{F_{cal} \cdot A_i} * 100$.

Subjects' inclusion and exclusion criteria

We compared the TU measurements on our CZT Gamma Camera with Planar, SPECT and SPECT/CT acquisition modes on a selected population of 23 patients. Twenty-three consecutive patients with hyperthyroidism, referred to our institution, were included in the study from October 2019 to June 2020. After the presumptive diagnosis was made, all subjects underwent a thyroid scintigraphy. Pregnancy was the exclusion criterion.

Our routine thyroid examination started with the planar acquisition 20 min after the injection and was followed immediately with a SPECT/CT acquisition. The $^{99m}TcO_4$ uptake was measured 20 min after tracer intravenous injection. Residual activities in the syringes after injection were considered. The reference activity of the injected $^{99m}TcO_4$ was 80 MBq.

Ethical approval was waived by the local Ethics Committee of our institution in view of the nature of the study and all the procedures being performed were part of the routine care. The retrospective study was registered with ClinicalTrials.gov number NCT05049551.

Statistical analysis

Measured data were provided as the mean \pm standard deviation (SD). Correlations of TU between Planar, Tomo-AC and Tomo-NoAC images and between theoretical and estimated AThA were assessed using the Pearson correlation coefficient (r). The difference was calculated between each of the TU measurements (Planar vs Tomo-AC, Planar vs Tomo-NoAC and Tomo-AC vs Tomo-NoAC) using a graphical Bland and Altman method. The graphical correlation analysis of the AThA was done individually on the five anthropomorphic 3D-thyroid phantoms. The relative percentage difference between theoretical and estimated AThA defined as $100 * (A_{ThA_{Estimated}} - A_{ThA_{Theoretical}}) / A_{ThA_{Theoretical}}$ for Planar, Tomo-AC and Tomo-NoAC were calculated for all the five anthropomorphic 3D-thyroid phantoms.

The upper and lower limits for the Bland and Altman plot analysis were calculated using $mean \pm 2 \times SD$. P value < 0.05 was considered statistically significant.

Dosimetry estimation

For each patient, the dosimetric information included the volume computed tomography dose index for body in mGy ($CTDI_{vol}$) and dose length product in mGy.cm (DLP) for the X-ray CT, and the activity injected of $^{99m}TcO_4$ (in MBq) for the scintigraphy.

Table 1 Cross-calibration factors for the planar, SPECT/CT and SPECT acquisitions

Acquisition	Cross-calibration factors (counts. MBq ⁻¹ s ⁻¹)
Type	Mean ± SD
Planar	66.2 ± 4.9
SPECT/CT (Tomo-AC)	60.7 ± 0.7
SPECT (Tomo-NoAC)	26.5 ± 0.3

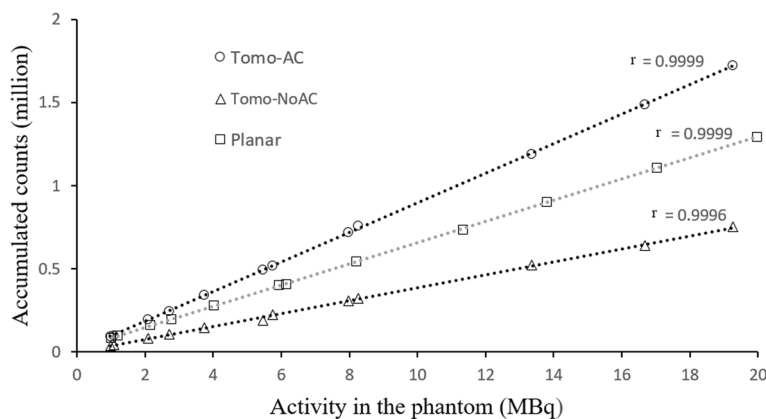


Fig. 3 Representation of the variation of the accumulated counts as a function of the activity in the vial ranging from 1 to 20 MBq for the SPECT/CT (Tomo-AC), SPECT (Tomo-NoAC) and Planar acquisitions

Effective dose (in Sv) and thyroid absorbed dose (in Gy) were calculated using International Commission on Radiological Protection (ICRP) reports 80 and 103 and the VirtualDoseTMCT software from Virtual Phantoms, Inc [22].

Results

Cross-calibration parameters of the CZT gamma camera

The cross-calibration factors for the three acquisition modes: Planar, Tomo-AC and Tomo-NoAC, are summarized in Table 1. To ensure the stability of these cross-calibration factors, several activities were studied corresponding to a range of 1–20 MBq (Fig. 3). We verified the linear correlation coefficient (*r*) as 0.9999 for Planar, 0.9999 for Tomo-AC and 0.9996 for Tomo-NoAC, which correspond to a perfect linearity.

Measurements of the absolute thyroid activity

To generate a geometric model of thyroid that represents a human thyroid as closely as possible, Planar (Fig. 4) and SPECT/CT (Fig. 5) images of the anthropomorphic phantoms were acquired. For all five thyroids phantoms, the estimated AThA was plotted in comparison with the theoretical AThA for the three acquisition modes, as illustrated in Fig. 6. The injected activity in the five thyroid phantoms ranged from 0.4 to 10 MBq.

The Pearson correlation coefficient *r* for the theoretical and estimated AThA for Planar, Tomo-AC and Tomo-NoAC images were statistically highly correlated (*r* < 0.99; *P* < 10⁻⁴).



Fig. 4 Planar scintigraphy of the 19 cc anthropomorphic thyroid phantom

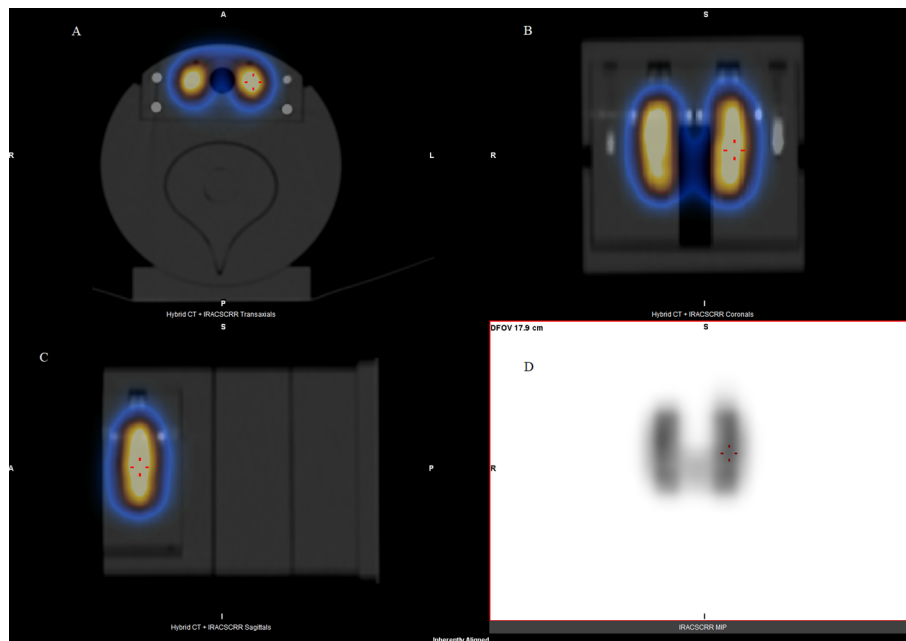


Fig. 5 SPECT/CT (A: transverse slice, B: coronal slice, C: frontal slice) fusion views and maximum intensity projection view (D) of the 19 cc anthropomorphic thyroid phantom

The average of the relative percentage difference between theoretical and estimated AThA for all the thyroid phantoms showed an excellent agreement and were for Planar, Tomo-AC and Tomo-NoAC images (8.6 ± 17.8), (-1.3 ± 5.2) and (12.8 ± 5.7), respectively.

Patients' description

The twenty-three patients included 10 females (44%) and 13 males (56%). Their mean age was 58.9 ± 17 years, with a range of 29–89 years. Their mean weight was 73.1 ± 19.3 kg, with a range of 48–112 kg. The mean net injected activity of $^{99m}\text{TcO}_4$ was 79.2 ± 3.7 MBq.

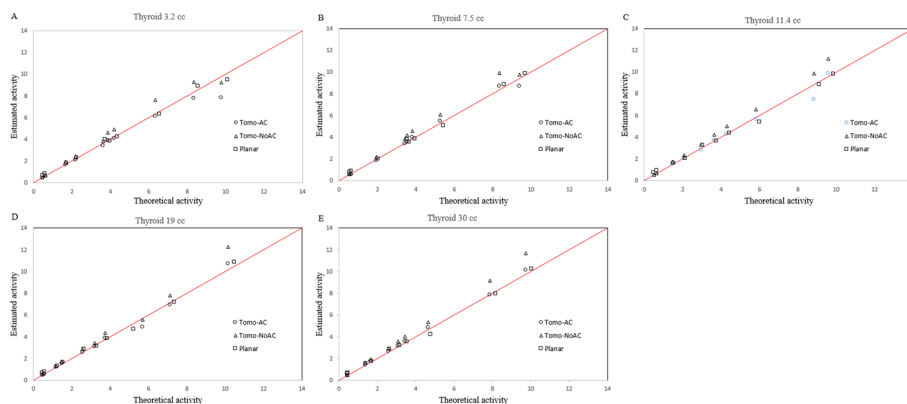


Fig. 6 Correlations curves (A, B, C, D and E) between theoretical and estimated activity of Tomo-AC, Tomo-NoAC and Planar acquisitions for anthropomorphic thyroid volumes of 3.2, 7.5, 11.4, 19 and 30 cc

Clinical results

Thirteen patients (56%) were found to have one or several hot nodules. Among this subset of patients, SPECT/CT was able to detect all nodules seen with planar images. It was easier to localize nodules with a 3D representation of the thyroid in SPECT/CT images than planar image, as illustrated in Fig. 7 of the same patient (case #23). In Fig. 7K, the planar scintigraphy indicates a pathological, principally a large hot nodule in the right para-isthmic region. SPECT/CT, in contrast, reveals not only the large right para-isthmic hot nodule, but also two additional areas of focal uptake in the upper pole of both lobes, which are consistent with hot nodules (Fig. 7A, B, C, D, E, F, G, H, I, J).

Measurements of the patients' thyroid uptake

Comparisons of TU between different pairs of images (Planar vs Tomo-AC, Planar vs Tomo-NoAC and Tomo-AC vs Tomo-NoAC) are shown in Fig. 8. Planar, SPECT/CT and SPECT images show statistically significant correlations ($r=0.972$, 0.961 and 0.935 , respectively; $P < 10^{-3}$). The Bland and Altman analysis, as represented in Fig. 9, indicates a good agreement of the calculated TU between the Planar versus Tomo-AC, Planar versus Tomo-NoAC and Tomo-AC versus Tomo-NoAC images, with a mean difference, respectively, of 0.338 (-0.563 to 1.239), -0.208 (-1.019 to 0.602) and 0.546 (-0.805 to 1.898).

Dosimetry results

Dosimetric information from CT and SPECT examinations of the 23 patients were used to calculate the thyroid absorbed dose. The mean activity of the injected $^{99m}\text{TcO}_4$ was 79.2 ± 3.7 MBq. The mean of the CTDI_{vol} and DLP were estimated at 2.21 ± 0.2 mGy and 49.5 ± 9 mGy.cm, respectively. The mean effective dose and the thyroid absorbed dose, for the CT and the nuclear medicine (NM) parts, were found to be $0.34_{\text{CT}} + 0.95_{\text{NM}}$ mSv and $3.88_{\text{CT}} + 1.75_{\text{NM}}$ mGy, respectively. All of these results are summarized in Table 2.

Discussion

In order to quantify $^{99m}\text{TcO}_4$ TU on planar, SPECT and SPECT/CT series using a large field of view CZT gamma camera, we first determined cross-calibration factors using a thyroid phantom. Then, the ATa was calculated for planar and SPECT/CT acquisitions

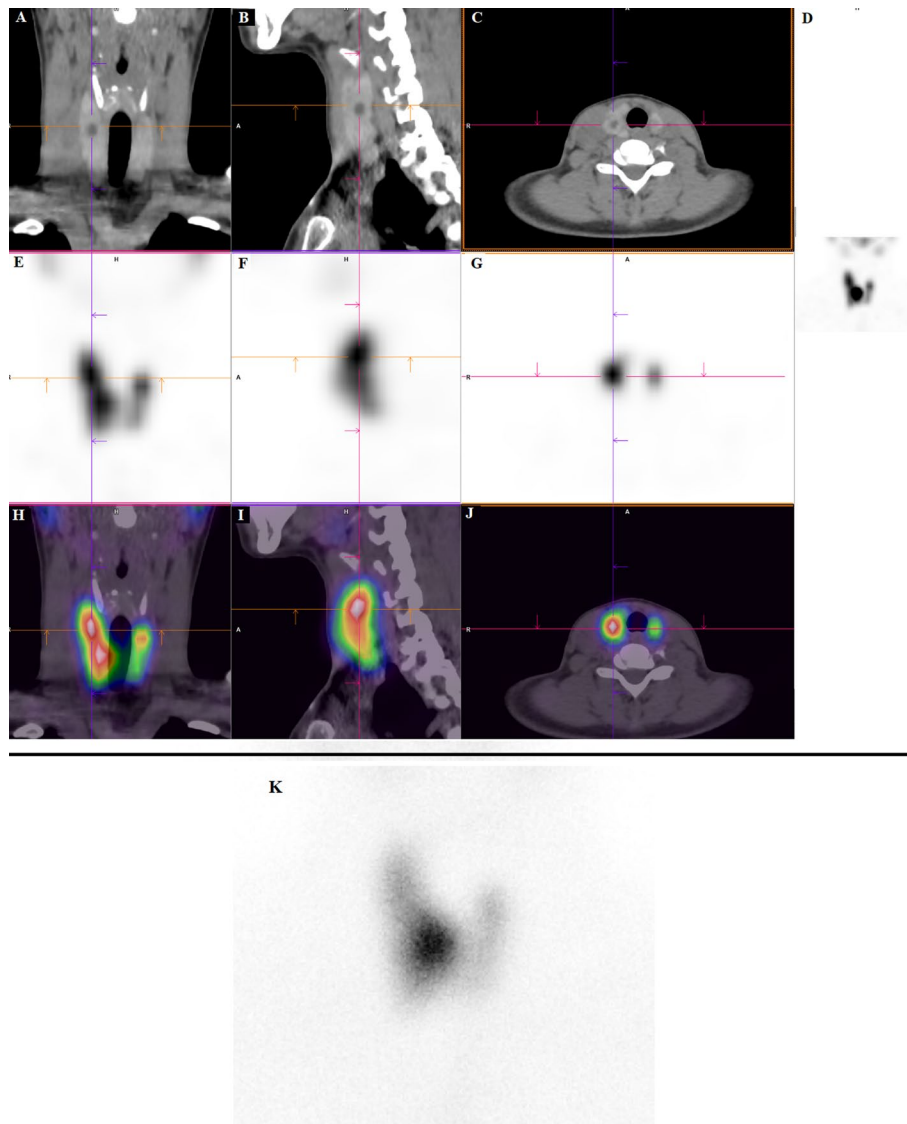


Fig. 7 CT, SPECT and fusion in, respectively, coronal (A, E, H), sagittal (B, F, I), transverse (C, G, J) images, MIP (D) and Planar scintigraphy (K) of patient case #23, showing for Planar mainly the hot right nodule and for SPECT/CT the same hot right nodule and also hot nodules in the upper pole of right and left lobes

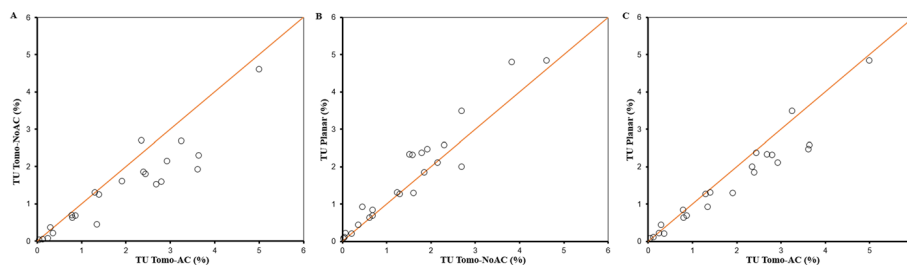


Fig. 8 Correlations between TU based on different pairs of images Tomo-AC versus Tomo-NoAC (A), Planar versus Tomo-NoAC (B) and Planar versus Tomo-AC (C)

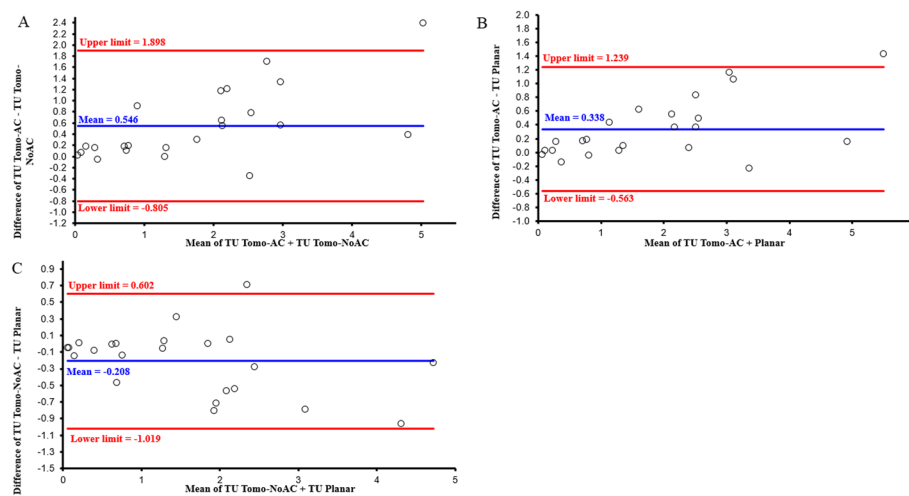


Fig. 9 Bland and Altman plot analysis of TU calculated between Tomo-AC versus Tomo-NoAC (A), Planar versus Tomo-AC (B), and Planar versus Tomo-NoAC (C) images

Table 2 Thyroid and effective dosimetry data of the 23 patients

	Mean	SD	Range
Injected Activity (MBq)	79.2	3.7	(71.5–86.7)
CTDI _{vol} (mGy) (body)	2.21	0.2	(1.6–2.5)
DL P(mGy cm)	49.5	9	(33–65)
CT-effective dose (mSv)*	0.34	0.03	(0.24–0.38)
^{99m} TcO ₄ -effective dose(mSv)**	0.95	0.04	(0.86–1.04)
CT-Thyroid absorbed dose (mGy)*	3.88	0.36	(2.82–4.38)
^{99m} TcO ₄ -thyroid absorbed dose (mGy)**	1.74	0.08	(1.57–1.91)

*ICRP-103 and Virtual-Phantoms, Inc. software, ** ICRP-80

on five anthropomorphic 3D thyroid phantoms, and the TU was calculated for the acquisitions performed on 23 consecutive patients. To our knowledge, the feasibility of such thyroid quantification using a large field of view CZT gamma camera has not been previously demonstrated in the literature.

The TU value obtained with planar acquisition after injection of ^{99m}TcO₄ is one of the parameters used in nuclear medicine for the diagnosis of thyroid diseases and for pathological follow-up. Its clinical value is limited, as it depends on many factors such as thyroid volume, patient's iodine supply, hormonal status and patient's age [3–5, 18, 23, 24]. Its use is recommended by the European Association of Nuclear Medicine (EANM) and the Society of Nuclear Medicine and Molecular Imaging (SNMMI) practice guideline for thyroid scintigraphy [18].

However, one of the main issues with this parameter is that its normal reference range is not clearly defined [25–30]. Estimated of TU and thyroid scintigraphy are established according to guidelines [18, 19] using planar acquisitions on a NaI scintillation detector equipped with an Anger-type gamma camera with parallel and pinhole collimators. The pinhole collimator is used just for diagnostics, but not for the estimation of TU. Attenuation correction (AC) and scatter correction (SC), resolution recovery (RR) and the iterative OSEM algorithm allow a quantitative SPECT/CT approach [12, 31–33], despite the

relatively poor spatial resolution and the partial volume effects that limit quantitation of radioactivity for objects smaller than three times the spatial resolution [34].

Ahmed et al. performed a bibliographic evaluation [35] with iodine-131 on hybrid SPECT/CT imaging compared to planar scintigraphy. The aim of that study was to treat differentiated thyroid carcinomas. The authors concluded that SPECT/CT was superior to planar in distinguishing pathologies from physiological uptake by increasing the accuracy of image interpretation. SPECT/CT improved the accuracy of differentiating the stages of thyroid cancer and subsequent patient management. Their conclusion was mainly based on the lack of anatomical detail in planar gamma camera images and the superimposition of areas leading to false positive results and potential to over-treat patients.

Zaidi [36] investigated comparative methods on a thyroid phantom to quantify thyroid volume using planar and SPECT imaging with technetium-99 m on a scintillation (NaI) gamma camera. He concluded that images from SPECT with attenuation and scatter corrections provided the most accurate determination of thyroid phantom volume, but failed at smaller volumes where errors caused by the partial volume effect were significant.

In contrast, Iizuka et al. [37], using iodine-131 scintigraphy, compared planar with SPECT images for quantification of radiation intensity, concluding that planar images provided better accuracy for determining the radiation dose. Their approach differed from ours and was based on an iodine-131 reference capsule placed next to the patient during image acquisition. Iodine-131, as a high photon energy radioisotope, has poor sensitivity to the gamma camera due to collimator penetration, a factor that could explain those results.

The CZT digital detector, based on cadmium zinc telluride technology, provides high resolution SPECT images by directly converting gamma radiation into an electrical signal. The high performance of the CZT detector with its specific acquisition and reconstruction parameters (WEHR collimator, energy window set at 15%, iterative reconstruction with AC, SC and RR corrections) provides several major advantages for our purpose. First, it was not necessary to increase the injected $^{99m}\text{TcO}_4$ activity while maintaining the quantitative accuracy of the SPECT and SPECT/CT image data [32]. Second, the high spatial and energy resolutions of the CZT, compared to the Anger camera, result in an improved image quality in terms of contrast and spatial resolution [17].

The perfect linearity of the change in accumulated counts as a function of activity for Planar, Tomo-AC and Tomo-NoAC images, with $r=0.9999$, 0.9999 and 0.9996 , respectively (Fig. 3), ensures the stability of the cross-calibration factors. Estimation of the AThA of the five anthropomorphic phantoms show evidence that the cross-calibration factors are validated for all five thyroid sizes (from 3.2 cc to 30 cc) and for variable activity in the phantoms ranging from 0.4 to 10 MBq, which represents the typical uptake of $^{99m}\text{TcO}_4$ activity in a patient thyroid.

The average of the relative percentage difference between theoretical and estimated AThA for all the thyroid phantoms showed an excellent agreement, particularly for the Tomo-AC, and were for Planar, Tomo-AC and Tomo-NoAC images (8.6 ± 17.8), (-1.3 ± 5.2) and (12.8 ± 5.7), respectively. The results in Figs. 8 and 9 show a good

agreement among the TU values calculated with planar and tomographic images using cross-calibration factors. In addition, the correlation between Planar versus Tomo-AC, Planar versus Tomo-NoAC and Tomo-AC versus Tomo-NoAC (Fig. 8) was excellent ($r=0.972, 0.961$ and 0.935 , respectively; $P < 10^{-3}$), offering the possibility of using either SPECT or SPECT/CT for TU quantifications. The thyroid's proximity to the skin, inducing a low level of attenuation and scattering, partly explains the excellent correlation values between Planar, SPECT and SPECT/CT images. In addition, SPECT imaged limited patient exposure compared to SPECT/CT.

Regarding the contribution of 3D imaging (Tomo-AC and NoAC), although it did not directly influence the therapeutic strategy in our 23 cases, a potential superiority of tomographic images in the detectability and localization of thyroid nodules in comparison with planar conventional acquisitions was evident. This finding is consistent with previous studies [12, 20, 31, 32, 35, 36, 38] that have demonstrated the utility of SPECT for accurate localization of thyroid tracer uptake. Clearly, the CT scan associated with SPECT enhances the anatomic localization of hot thyroid nodules and could likely be relevant to patient care.

A factor of consideration in this study's procedure is the potential radiation exposure to patients with CT acquisitions, especially for the thyroid glands. Nonetheless, in our configuration of a CZT coupled with an efficient CT scan, we were able to inject a low activity of $^{99m}\text{TcO}_4$ around 79.2 ± 3.7 MBq. Using low activity was possible due to the high performance of the CZT technology, along with specific SPECT reconstruction parameters and corrections. In addition, we used a low tube voltage (100 kVp) and the CT reducing methods such as current modulation (smart mA) and iterative CT reconstruction (ASIR).

The estimated effective dose of the patients was 1.29 mSv: 0.34 mSv for CT plus 0.95 mSv for the injection of $^{99m}\text{TcO}_4$. This is an acceptable effective dose, considering that the annual individual exposure among the population in France is 4.5 mSv [39] and the typical effective dose of an abdomen CT is 8.1 mSv [40]. However, the total organ absorbed dose for the thyroid was 5.63 mGy: 3.88 mGy for CT plus 1.74 mGy for the injection of $^{99m}\text{TcO}_4$ which should definitely motivate to reduce radiation exposure, especially for CT.

Conclusion

Using CZT technology, cross-calibration factors, validated through anthropomorphic thyroid phantoms using the same acquisition conditions as the patients, provide the ability to validate the TU value on a small series of patients with SPECT and SPECT/CT images. The Planar gold standard acquisition for TU could be substituted by SPECT or SPECT/CT acquisitions.

Although CT for AC reduces the errors on estimated AThA as compared to no AC and CT combined with SPECT enhances the anatomic localization of hot thyroid nodules, the additional value of combined CT remains to be confirmed in larger studies and involves an increase in the exposure. Patient radiation exposure remains a concern, especially because the thyroid is considered as a highly sensitive organ to ionizing radiation.

Abbreviations

AC	Attenuation correction
A_i	Activity injected to the patient
ANSI	American National Standards Institute
ASIR	Adaptive statistical iterative reconstruction
A_{th}	Activity measured in the thyroid
ATHA	Absolute thyroid activity
CT	X-ray commuted tomography
CTDI	Computed tomography dose index
CZT	Cadmium Zinc Telluride
DLP	Dose length product
EANM	European Association of Nuclear Medicine
F_{cal}	Cross-calibration factor
Gy	Gray
IAEA	International Atomic Energy Agency
ICRP	International Commission on Radiological Protection
MIP	Maximum Intensity Projection
$N_{ROI,th}$	Regions of interest counts in thyroid
OSEM	Ordered subsets expectation minimization
PET	Positron emission tomography
P_{max}	Maximum counts in a voxel (or pixel) within the region
r	Pearson correlation coefficient
ROIs	Regions of interest
ROI_{back}	Background region of interest
RR	Recovery reconstruction
SC	Scatter correction
SD	Standard deviation
SNMMI	Society of Nuclear Medicine and Molecular Imaging
SPECT	Single photon emission computed tomography
Sv	Sievert
Tomo-AC	Tomography with attenuation correction
Tomo-NoAC	Tomography without attenuation correction
TU	Thyroid uptake
VOIs	Volumes of interest
VS	Versus
WEHR	Wide Energy High Resolution

Acknowledgments

Not applicable.

Author contributions

BS, TB and BP designed and supervised the study. BS, RA, FH, MD, NG, RV, VN, FM, CM, MF and BP contributed to acquisition and imaging processing data. BS and FB performed statistical analysis. BS, RA, TB and BP wrote the manuscript. RA, FH, MD, FB, NG, RV, VN, FM, CM and MF contributed to critical revision of the report. All authors read and approved the final draft of the manuscript.

Funding

No funds were received for this work.

Availability of data and materials

The datasets used and analyzed during this current study are available from the corresponding author upon reasonable request.

Declarations**Ethics approval and consent to participate**

All the retrospective procedures performed in this study involving human data were approved by the Princess Grace Hospital clinical research steering committee. All procedures in this study involving human data were performed in accordance with the regulatory and ethical standards. "Comité de Pilotage de la recherche du Centre Hospitalier Princesse Grace" (Pilot committee for research of Centre Hospitalier Princesse Grace) was the institutional review board that approved the study.

Consent for publication

All subjects gave informed consent to allow their clinical data to be used for retrospective additional research and publication.

Competing of interests

The authors declare that they have no competing interests.

Received: 3 April 2023 Accepted: 24 July 2023

Published online: 31 July 2023

References

1. Atkins H, Fleay R. Data blending with ^{99m}Tc in evaluating thyroid anatomy by scintillation scanning. *J Nucl Med*. 1968;9(2):66–73.
2. Atkins H, Klopper J. Measurement of thyroidal technetium uptake with the gamma camera and computer system. *Am J Roentgenol Radium Ther Nucl Med*. 1973;118(4):831–5.
3. Schneider P. Simple, rapid thyroid function testing with ^{99m}Tc -pertechnetate thyroid uptake ratio and neck/thigh ratio. *Am J Roentgenol*. 1979;132(2):249–53.
4. Selby JB, Buse MG, Gooneratne NS, Moore DO. The anger camera and the pertechnetate ion in the routine evaluation of thyroid uptake and imaging. *Clin Nucl Med*. 1979;4(6):233–7.
5. Sucupira MS, Camargo EE, Nickloff EL, Alderson PO, Wagner HN Jr. The role of ^{99m}Tc pertechnetate uptake in the evaluation of thyroid function. *Int J Nucl Med Biol*. 1983;10(1):29–33. [https://doi.org/10.1016/0047-0740\(83\)90030-x](https://doi.org/10.1016/0047-0740(83)90030-x).
6. Becker D, Charkes ND, Dworkin H, et al. Procedure guideline for thyroid uptake measurement: 1.0. Society of nuclear medicine. *J Nucl Med*. 1996;37(7):1266–8.
7. Ramos CD, Wittmann D, Sa de Camargo Etchebehere EC, Tambascia M, Moreira Silva CA, Camargo EE. Thyroid uptake and scintigraphy using ^{99m}Tc pertechnetate: standardization in normal individuals. *Sao Paulo Med J*. 2002;120(2):458. <https://doi.org/10.1590/s1516-31802002000200004>.
8. Gulec S, Kuker RA, Goryawala M, et al. (124) PET/CT in patients with differentiated thyroid cancer: clinical and quantitative image analysis. *Thyroid*. 2016;26(3):441–8. <https://doi.org/10.1089/thy.2015.0482>.
9. Wu D, Ylli D, Heimlich SL, Burman KD, Wartofsky L, Van Nostrand D. ^{124}I Positron emission tomography/computed tomography versus conventional radioiodine imaging in differentiated thyroid cancer: a review. *Thyroid*. 2019;29(11):1523–35. <https://doi.org/10.1089/thy.2018.0598>.
10. Darr AM, Opfermann T, Nicksch T, Driesch D, Marlowe RJ, Freesmeyer M. Low-activity ^{124}I -PET/low-dose CT versus ^{99m}Tc -pertechnetate planar scintigraphy or ^{99m}Tc -pertechnetate single-photon emission computed tomography of the thyroid: a pilot comparison. *Clin Nucl Med*. 2013;38(10):770–7. <https://doi.org/10.1097/RLU.0b013e3182a20d26>.
11. Ritt P, Vija H, Hornegger J, Kuwert T. Absolute quantification in SPECT. *Eur J Nucl Med Mol Imaging*. 2011;38(Suppl 1):S69–77. <https://doi.org/10.1007/s00259-011-1770-8>.
12. Lee H, Kim JH, Kang Y, Moon JH, So Y, Lee WW. Quantitative single-photon emission computed tomography/computed tomography for technetium pertechnetate thyroid uptake measurement. *Medicine*. 2016;95(27):e4170. <https://doi.org/10.1097/MD.00000000000004170>.
13. Gnesin S, Ferreira PL, Malterre J, Laub P, Prior JO, Verdun FR. Phantom validation of Tc-99m absolute quantification in a SPECT/CT commercial device. *Comput Math Methods Med*. 2016;2016:4360371. <https://doi.org/10.1155/2016/4360371>.
14. Halty A, Badel JN, Kochebina O, Sarrut D. Image-based SPECT calibration based on the evaluation of the fraction of activity in the field of view. *Eur J Nucl Med Mol Imaging Phys*. 2018;5(1):11. <https://doi.org/10.1186/s40658-018-0209-8>.
15. Druz RS, Phillips LM, Chugkowski M, Boutis L, Rutkin B, Katz S. Wide-beam reconstruction half-time SPECT improves diagnostic certainty and preserves normalcy and accuracy: a quantitative perfusion analysis. *J Nucl Cardiol*. 2011;18(1):52–61. <https://doi.org/10.1007/s12350-010-9304-5>.
16. Enevoldsen LH, Menashi CAK, Andersen UB, Jensen LT, Henriksen OM. Effects of acquisition time and reconstruction algorithm on image quality, quantitative parameters, and clinical interpretation of myocardial perfusion imaging. *J Nucl Cardiol*. 2013;20(6):1086–92. <https://doi.org/10.1007/s12350-013-9775-2>.
17. Ito T, Matsusaka Y, Onoguchi M, Ichikawa H, Okuda K, Shibutani T, Shishido M, Sato K. Experimental evaluation of the GE NM/CT 870 CZT clinical SPECT system equipped with WEHR and MEHRs collimator. *J Appl Clin Med Phys*. 2021;22(2):165–77. <https://doi.org/10.1002/acm2.13158>.
18. Giovanella L, Avram A, Iakovou I, et al. EANM practice guideline/SNMMI procedure standard for RAIU and thyroid scintigraphy. *Eur J Nucl Med Mol Imaging*. 2019;46(12):2514–25. <https://doi.org/10.1007/s00259-019-04472-8>.
19. Mariani G, Tonacchera M, Grosso M, Orsolini F, Vitti P, Strauss HW. The role of nuclear medicine in the clinical management of benign thyroid disorders, Part 1: hyperthyroidism. *J Nucl Med*. 2021;62(3):304–12. <https://doi.org/10.2967/jnumed.120.243170>.
20. Dong F, Li L, Bian Y, Li G, Han X, Li M, Liu J, Xue Y, Li Y, Hu Y, Tan J. Standardized uptake value using thyroid quantitative SPECT/CT for the diagnosis and evaluation of graves' disease: a prospective multicenter study. *Biomed Res Int*. 2019;2019:7589853. <https://doi.org/10.1155/2019/7589853>.
21. Beaumont T, Ideias CP, Rimlinger M, Broggio D, Franck D. Development and test of sets of 3D printed age-specific thyroid phantoms for ^{131}I measurements. *Phys Med Biol*. 2017;62(12):4673–93. <https://doi.org/10.1088/1361-6560/aa6514>.
22. Ding A, Gao Y, Liu H, Caracappa P, Long D, Bolch W, Liu B, Xu G. VirtualDose: a software for reporting organ doses from CT for adult and pediatric patients. *Phys Med Biol*. 2015;60(14):5601–25. <https://doi.org/10.1088/0031-9155/60/14/5601>.
23. Meller J, Becker W. Scintigraphic evaluation of functional thyroidal autonomy. *Exp Clin Endocrinol Diabetes*. 1998;106(Suppl 4):S45–51. <https://doi.org/10.1055/s-0029-1212056>.
24. Meller J, Becker W. The continuing importance of thyroid scintigraphy in the era of high-resolution ultrasound. *Eur J Nucl Med*. 2002;29(Suppl 2):S425–38. <https://doi.org/10.1007/s00259-002-0811-8>.
25. Fadime D. Cut off value of technetium uptake in the differential diagnosis of Graves, disease and subacute thyroiditis. *Asia Ocean J Nucl Med Biol*. 2020;8(1):54–7. <https://doi.org/10.22038/aojnmb.2019.14241>.
26. Macauley M, Shawgi M, Ali T, et al. Assessment of normal reference values for thyroid uptake of technetium-99m pertechnetate in a single centre UK population. *Nucl Med Commun*. 2018;39(9):834–8. <https://doi.org/10.1097/mnm.0000000000000876>.
27. Wang C, Zhao Y, Shen Y. Inaccuracy of thyroid to background uptake ratio in evaluating technetium-99m-pertechnetate thyroid uptake and establishing an improved algorithm. *Asia Ocean J Nucl Med Biol*. 2019;7(2):160–71. <https://doi.org/10.22038/aojnmb.2019.12734>.

28. Alshahrani A, Syed GM, Khan AH, et al. Assessment of normal reference values for thyroid uptake of technetium-99m pertechnetate in a Saudi population. *Ann Saudi Med*. 2021;41(2):86–90. <https://doi.org/10.5144/0256-4947.2021.86>.
29. Abdelhamed H, Abdo Soliman M, Mahmoud A, Mohamed R, Ali I, Abdelhai S. The utility of technetium-99m pertechnetate thyroid scintigraphy assessing thyroid/salivary ratio as an alternative to thyroid uptake percentage in evaluation of thyroid function, with establishing normal reference values of both parameters: single Egyptian center study. *Nucl Med Commun*. 2022;43(12):1181–7. <https://doi.org/10.1097/MNM.0000000000001620>.
30. Meihua J, Jonghwa A, Seong-gil J, et al. Comparison of Tc-99m pertechnetate thyroid uptake rates by gamma probe and gamma camera methods for differentiating Graves' disease and thyroiditis. *Nucl Med Mol Imaging*. 2022;56(1):42–51. <https://doi.org/10.1007/s13139-021-00734-2>.
31. Kim JY, Kim JH, Moon JH, et al. Utility of quantitative parameters from single-photon emission computed tomography/computed tomography in patients with destructive thyroiditis. *Korean J Radiol*. 2018;19(3):470–80. <https://doi.org/10.3348/kjr.2018.19.3.470>.
32. Lee WW, K-SPECT Group. Clinical applications of technetium-99m quantitative single-photon emission computed tomography/computed tomography. *Nucl Med Mol Imaging*. 2019;53:172–81. <https://doi.org/10.1007/s13139-019-00588-9>.
33. Dickson JC, Armstrong IS, Gabiña PM, et al. EANM practice guideline for quantitative SPECT-CT. *Eur J Nucl Med Mol Imaging*. 2023;50(4):980–95. <https://doi.org/10.1007/s00259-022-06028-9>.
34. Bailey DL, Willowson KP. An evidence-based review of quantitative SPECT imaging and potential clinical applications. *J Nucl Med*. 2013;54(1):83–9. <https://doi.org/10.2967/jnumed.112.111476>.
35. Ahmed N, Niyaz K, Borakati A, Marafi F, Birk R, Usmani S. Hybrid SPECT/CT imaging in the management of differentiated thyroid carcinoma. *Asian Pac J Cancer Prev*. 2018;19(2):303–8. <https://doi.org/10.22034/APJCP.2018.19.2.303>.
36. Zaidi H. Comparative methods for quantifying thyroid volume using planar imaging and SPECT. *J Nucl Med*. 1996;37(8):1421–6.
37. Iizuka Y, Katagiri T, Inoue M, Nakamura K, Mizowaki T. Comparison between planar and single-photon computed tomography images for radiation intensity quantification in iodine-131 scintigraphy. *Sci Rep*. 2021;11(1):21858. <https://doi.org/10.1038/s41598-021-01432-x>.
38. Freesmeyer A, Winkens T, Kühnel C, Opfermann T, Seifert P. Technetium-99m SPECT/US hybrid imaging compared with conventional diagnostic thyroid imaging with scintigraphy and ultrasound. *Ultrasound Med Biol*. 2019;45(5):1243–52. <https://doi.org/10.1016/j.ultrasmedbio.2019.01.003>.
39. Institute for Radiological Protection and Nuclear Safety (IRSN). Exposure of the French population to ionizing radiation, 2014–2019 report. <https://search.proquest.com/openview/60871b577951075aad5d8938b31fcd44/1?pq-origsite=gscholar&cbl=40808>
40. Vilar-Palop J, Vilar J, Hernandez-Aguado I, Gonzalez-Alvarez I, Lumberras B. Update effective dose in radiology. *J radiolog Prot*. 2016;36(4):975–90. <https://doi.org/10.1088/0952-4746/36/4/975>.

Publisher's Note

Springer Nature remains neutral with regard to jurisdictional claims in published maps and institutional affiliations.

Submit your manuscript to a SpringerOpen[®] journal and benefit from:

- Convenient online submission
- Rigorous peer review
- Open access: articles freely available online
- High visibility within the field
- Retaining the copyright to your article

Submit your next manuscript at ► [springeropen.com](https://www.springeropen.com)
